Research article

Effects of different quantities of antibody conjugated with magnetic nanoparticles on cell separation efficiency

Amir Hossein Haghighi [a], Mohammad Taghi Khorasani [b], Zahra Faghih [c,*], Fatemeh Farjadian [d]

[a] Department of Biomedical Engineering, Science and Research Branch, Islamic Azad University, Tehran, Iran
[b] Biomaterials Department, Iran Polymer and Petrochemical Institute, Tehran, Iran
[c] Shiraz Institute for Cancer Research, Medical School, Shiraz University of Medical Sciences, Shiraz, Iran
[d] Pharmaceutical Sciences Research Center, Faculty of Pharmacy, Shiraz University of Medical Sciences, Shiraz, Iran

ABSTRACT

Antibody-conjugated magnetic nanoparticles (Ab-MNPs) have received considerable attention in bioseparation and clinical diagnostics assays due to their unique ability to detect and isolate a variety of biomolecules and cells. Because antibodies can be expensive, a key challenge for bioconjugation is to determine the optimal amount of antibodies with reasonable antigen-capturing activity. We designed an approach to determine the minimum amounts of antibodies for efficient coating. Different quantities of Herceptin (anti-human epidermal growth factor receptor 2: HER2) antibody were applied and immobilized on the surface of MNPs. Antibody binding was then checked by using an anti-human antibody conjugated with fluorochrome and flow cytometry. When the ratio of MNPs to antibodies increased from 0.79 to 795.45, mean fluorescence intensity (MFI) of conjugated MNPs decreased markedly from 185.56 to 20.07, indicating lower surface antibody coverage. We then investigated the relation between antibody content and isolation efficiency. Three Ab-MNP samples with different MFI were used to isolate SK-BR-3, a HER2-positive breast cancer cell line, from mixtures of whole blood or mononuclear cells. After isolation in a magnetic field, separation efficiency was evaluated by fluorescence microscopy and flow cytometry-based techniques. Our results collectively showed that the amount of anti-HER2 antibodies for conjugation with MNPs could be decreased by as much as one-fifteenth without compromising isolation efficiency, which in turn can reduce the cost of immunoassay biosensors.

1. Introduction

The ability of antibodies (Abs) to bind to specific antigens is an area of interest in efforts to target cellular and molecular markers, particularly in the context of diagnostics and therapeutic applications [1, 2, 3]. An innovative approach in antibody-based capture assays is their immobilization on the surface of nanoparticles to exploit their unique nanoscale properties. A variety of nanoparticles including polymers [4], gold nanoparticles [5], quantum dots [6], silica nanoparticles [7] and magnetic nanoparticles (MNPs) [8] have been used to obtain conjugates with Abs.

MNPs have shown promise in biotechnology due to their low toxicity, superparamagnetism, high surface area and simple separation [9, 10, 11, 12]. While, the high viscosity and large sizes of microbeads prevented their efficient interaction with cell surfaces, the higher surface area rather than microparticles and an efficient nano sizes of nanoparticles

facilitate the bioseparation and purification of a variety of bio-macromolecules and cells [13] including proteins [14], nucleic acids [15], viruses [16], bacteria [17, 18], and cancerous cells [19]. They have also been applied for drug delivery [20, 21], magnetic resonance imaging [22, 23, 24, 25], hyperthermia [26], diagnosis and treatment in various cancers [27, 28, 29, 30], and magnetic separation [31, 32].

In most cases, MNPs for specific targeting are coated with Abs. The main parameters which should be considered in the performance and targeting capability of these MNPs are the orientation of Abs on the surface, the immobilization strategy, and the antibody load [33]. Ideally, to ensure accessibility of the antigen binding fragment (Fab), Abs should be conjugated on the surface through their fragment crystallizable (Fc) region, which makes the Fab region available for antigen recognition, as explained in an earlier publication [34]. Another key parameter is surface density (which has been shown to provide an accurate) estimate of antibody activity [33, 35]. In this regard and in an experimental set-up,

---

* Corresponding author.
E-mail address: faghihz@sums.ac.ir (Z. Faghih).

Saha et al. immobilized several concentrations of anti-troponin Ab on the surface of MNPs and compared their antigen-capturing capacities in undiluted blood. Their results indicated that for optimal antigen-capturing activity, antibody concentration should be lower than those which led to a tightly packed layer [36]. Similarly, Puertas et al. also showed that higher antibody density on the surface had a negative impact on antigen-binding activities [37]. Despite these findings, orientation and density have not been studied in depth for many Abs. The available data for antibody conjugation specifically for human epidermal growth factor receptor 2 (HER2) on the surface of MNPs have been obtained mostly with specific amounts of antibodies [13, 38, 39, 40], but to the best to our knowledge data are still lacking for comparisons of different amounts of Abs on the surface of MNPs and their effects on antibody activities.

HER2, which is overexpressed in 10–25% of breast cancers, has become an area of interest in the detection of cancer cells [41]. The available data on antibody binding specifically on the surface of MNPs have been obtained mostly with specific amounts of anti-HER2 [13,39, 40]. Therefore, the present study was designed to develop a strategy to modify the MNP surface with amine groups in order to facilitate conjugation with the C-terminal region of Abs via ethyl-3-(3-dimethylaminopropyl)-carbodiimide (EDC)/N-hydroxysuccinimide (NHS) chemistry. We then used flow cytometry as a fast and reliable technique to assess the efficiency of Ab coating. In addition, we evaluated the effect of different amounts of Abs on the surface of MNPs on the separation efficiency of HER2+ breast cancer cells (SK-BR-3) to determine the optimal amount of anti-HER2 for conjugation without compromising antigen-capturing activity, with a view to devise cost-effective immunomagnetic platforms.

2. Materials and methods

2.1. Chemicals and reagents

Iron oxide MNPs (Fe_3O_4), 20–30 nm in diameter, 98% purity and coated with 1% polyvinylpyrrolidone (PVP) were purchased from US Research Nanomaterials, Inc. (USA). Herceptin was purchased from Roche (Germany). (3-aminopropyl) trimethoxysilane (APTMS), N-ethyl-N′-(3-dimethylaminopropyl) carbodiimide hydrochloride (EDC), and N-hydroxysuccinimide (NHS) were obtained from Sigma Aldrich (Germany). Phycoerythrin (PE)-conjugated mouse anti-human epithelial cell adhesion molecule (PE-anti-EpCAM) and fluorescein isothiocyanate (FITC)-conjugated mouse anti-human IgG antibody were provided by BD Biosciences (USA). Conjugated anti-human CD45 antibody (FITC-anti CD45) and 7-amino-actinomycin D (7-AAD) were obtained from Bio-Legend (USA). Carboxyfluorescein succinimidyl ester (CFSE) was purchased from Invitrogen (USA). Materials for cellular studies including fetal bovine serum (FBS), trypsin-EDTA (0.25%), penicillin-streptomycin and RPMI-1640 were purchased from Biosera (France). The human breast cancer cell line SK-BR-3 was obtained from the Pasteur Institute of Iran (Tehran, Iran). All chemicals were used directly without any further purification unless otherwise stated.

2.2. Functionalization of MNPs

MNPs underwent surface functionalization to provide amine groups (-NH2) on their surface to covalently bind to carboxyl groups (-COOH) of the Abs. Accordingly, we used APTMS for MNP coating with silane as previously reported [34, 42]. Briefly, 1 g MNPs was sonicated in 50 mL dried toluene; then 4 mL APTMS was added to the mixture, stirred at 80 °C under reflux condensation, and left to react for 4 days. The MNPs were then collected with an external magnet and washed thoroughly three times with acetone and ethanol. Silane-coated MNPs were obtained after vacuum drying at 50 °C within 24 h. A schematic of the experimental procedure is shown in Figure 1. The coating was then evaluated through different techniques as reported in our previous study [34]. The size and morphology of silane-coated MNPs were also examined with transmission electron microscopy (TEM) (Philips, model CM10, Netherlands). The slightly larger size (around 50 nm) compared to naked MNPs (20–30 nm as reported by the manufacturer) confirmed appropriate coating of MNPs with APTMS (Figure 2). The zeta potential of different samples was measured with a zeta potential analyzer (Microtrac, USA) at room temperature after dilution and sonication in deionized water (pH = 7) prior to measurement.

2.3. Conjugation of MNPs with Herceptin

Covalent coupling of Herceptin to amino-functionalized MNPs was followed by the procedure described previously [34]. Briefly, to activate Herceptin, NHS (12 mg, 0.1 mol) and EDC (8 mg, 0.04 mol) were
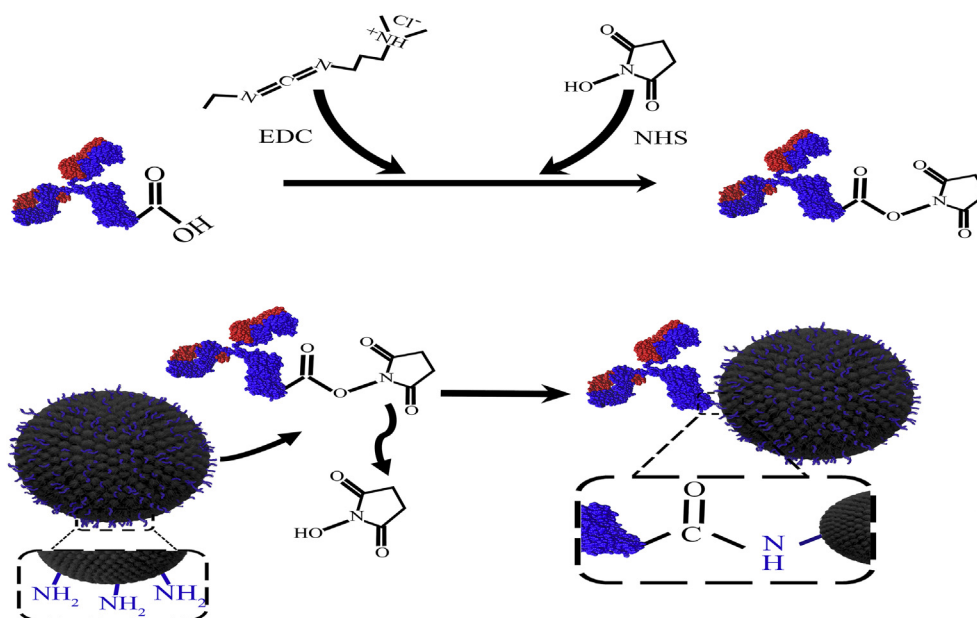
Figure. 1. Schematic of antibody immobilization on the surface of amine-modified magnetic nanoparticles via EDC/NHS chemistry.
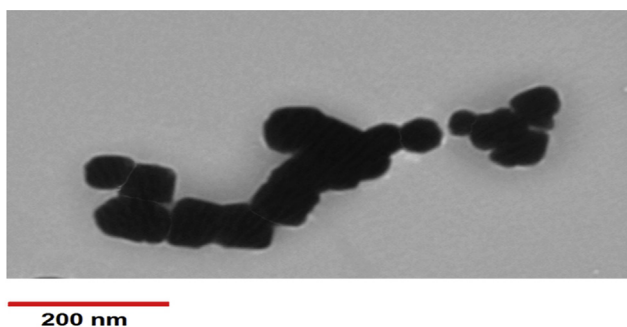
Figure 2. Transmission electron microscopic image of magnetic nanoparticles coated with silane.

Table 2. Zeta potentials of different magnetic nanoparticles.

Sample name	Zeta potential (mV)
MNPs	−72.6 ± 1.5
MNPs coated with silane	−56.4 ± 0.1
T17 (2.2 mg Ab)	−69.1 ± 0.9
T19 (0.55 mg Ab)	−63.2 ± 0.5
T25 (0.009 mg Ab)	−59.2 ± 0.6

MNPs: magnetic nanoparticles, Ab: antibody.

dissolved in 50 µL deionized water and added to different amounts of Herceptin at a concentration of 22 mg/mL (Table 1). MNPs (0.7 mL, 2.5 mg/mL) were then mixed with activated Herceptin and stirred continuously for 4 h at room temperature. The solution was washed three times with PBS 1× to elute EDC/NHS and unreacted Abs, then purified on a magnetic separator with a magnetic gradient of 0.5 T/m for 15–20 min. Finally, Ab-MNP conjugates were resuspended in storage buffer (PBS 1× containing 0.1 % FBS and 0.05 % sodium azide) at a concentration of 0.9 mg/mL.

2.4. Analyzing the conjugation of antibody to MNPs

To verify attachment of the Herceptin to MNPs, flow cytometry and energy dispersive X-ray spectroscopy (EDX) (Tescan VEGA3 instrument, Czech Republic) were used as previously described [34]. For flow cytometry assessment, Ab-MNP conjugates were first incubated on ice and ultrasonicated at a frequency of 15–20 kHz for 1 min (10 s off, 10 s on). Then a volume of 40 µL sonicated Ab-MNP conjugates was placed in a flow cytometry tube, stained with FITC mouse anti-human IgG antibody, and stored in the dark for 20 min at room temperature. A tube containing unconjugated MNPs was also used as a negative control. The tubes were washed with 2 mL PBS 1× and centrifuged at 300× g for 5 min. Cell populations were then acquired on a FACSCalibur flow cytometer (BD Biosciences, USA). Antibody binding to MNPs was also assessed with Fourier transform infrared spectroscopy (FTIR) (Bruker VERTEX 70v spectrophotometer, USA) and a zeta potential analyzer (Microtrac).

2.5. Cell culture

The human breast cancer cell line SK-BR-3 was cultured in culture flasks containing RPMI-1640 medium supplemented with 20% heat-inactivated FBS and 1% streptomycin/penicillin (10,000 units/mL, 10 mg/mL). The cells were then kept under a 5% CO_2 humidified atmosphere at 37 °C in a cell culture incubator. When the cells reached 80% confluency, they were treated with 0.25 trypsin/EDTA solution,

harvested, resuspended in fresh medium and prepared for testing. To measure cell viability, 10 µL of the cell suspension was mixed with 10 µL trypan blue dye and applied on a hemocytometer. The number of viable cells was then recorded under an inverted microscope as a shiny unstained cells.

2.6. Isolation of SK-BR-3 cells from a mixture of peripheral blood mononuclear cells

We then used a flow cytometry-based technique to evaluate the efficiency of Ab-MNP conjugates in the separation of SK-BR-3 cells from a mixture of peripheral blood mononuclear cells (PBMCs). Ultrasonicated Ab-MNPs (20 µL) were added to a suspension of 4×10^5 SK-BR-3 cells mixed with 2×10^6 PBMCs in a total volume of 100 µL (isolated by Ficoll-Hypaque density gradient) and incubated for 2 h at room temperature with stirring. The PBMCs and unreacted SK-BR-3 cells were then washed out 3 times with PBS 1× on the magnet for 15 min. For each reaction, similar tubes without magnetic separation were used simultaneously as controls. To assess the phenotype of captured cells, 10 µL PE-anti-EpCAM and FITC-anti-CD45 was added to both experimental and control tubes, which were then stored in the dark for 20 min at room temperature. After
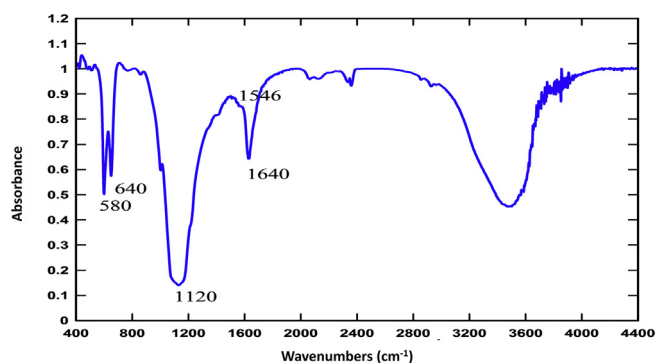
Figure 3. FTIR spectra of magnetic nanoparticles coated with silane (MNP) and magnetic nanoparticles conjugated with Herceptin antibody (sample T19 with 0.55 mg Herceptin).

Table 1. Characterization of magnetic nanoparticles conjugated with different amounts of Herceptin.

MNPs name	MNPs volume (µL)	MNPs weight (mg)	Ab volume (µL)	Ab weight (mg)	MFI	Ratio of MNPs to Ab
T17	700	1.75	100.00	2.20	185.56 ± 10.42	0.79
T19	700	1.75	25.00	0.55	110.19 ± 14.71	3.18
T21	700	1.75	6.25	0.143	90.10 ± 12.17	12.24
T23	700	1.75	1.56	0.036	80.17 ± 10.55	48.61
T25	700	1.75	0.39	0.009	51.75 ± 10.12	198.86
T27	700	1.75	0.09	0.002	20.07 ± 5.17	795.45

MNPs: magnetic nanoparticles, Ab: antibody, MFI: mean fluorescence intensity.

MNP

Element (MNP)	Error	W %	A %
C	16.66	4.6	9.74
N	0.00	0.00	0.00
O	17.21	40.70	64.74
Si	0.23	0.41	0.37
S	17.13	1.04	0.83
Ca	0.28	0.38	0.24
Mg	0.00	0.00	0.00
Fe	0.86	52.87	24.09
		100.00	100.00

T17

Element (T17)	Error	W %	A %
C	23.23	9.53	15.12
N	18.42	6.52	8.87
O	15.75	52.86	64.63
Si	26.02	0.72	0.49
S	14.19	4.14	1.83
Fe	0.79	26.23	9.06
		100.00	100.00

T19

Element (T19)	Error	W %	A %
C	10.11	7.19	13.20
N	10.28	3.73	5.85
O	10.45	45.83	63.12
Si	26.22	0.64	0.50
S	13.54	1.73	1.19
Fe	1.00	40.88	16.13
		100.00	100.00

Figure 4. EDX spectrum of magnetic nanoparticles coated with different amounts of Herceptin.

washing with 2 mL PBS 1× (650 ×g for 5 min), the cells were stained with 10 μL 7-AAD to exclude dead cells and incubated for 10 min in the dark at room temperature. Finally, 300 μL PBS 1× was added to all tubes, and cell populations were acquired on a four-color FACSCalibur flow cytometer (BD Biosciences).

2.7. Isolation of SK-BR-3 cells from a mixture of fresh human whole blood

To compare the experimental results with a real-life situation, we also assessed the efficiency of Ab-MNP conjugates in isolating SK-BR-3 cells from a mixture of fresh human whole blood. For this purpose, SK-BR-3 cells were pre-labeled with CFSE according to the manufacturer's staining protocol. As a live cell-staining fluorescent dye, CFSE changes the color of cells to green under fluorescent light. Then 1×10^5 CSFE-labeled SK-BR-3 cells was spiked into 1 mL fresh human whole blood and incubated with 90 μL Ab-MNPs, with stirring for 1 h at room temperature. After that a magnet was applied on sample tubes to isolate target cells from whole blood. After 15 min of magnetic separation, the supernatant was discarded, and the cells attached to the tube were carefully collected. The pellet was resuspended in 100 μL PBS 1× and examined with fluorescence microscopy (Olympus BX61, Japan).
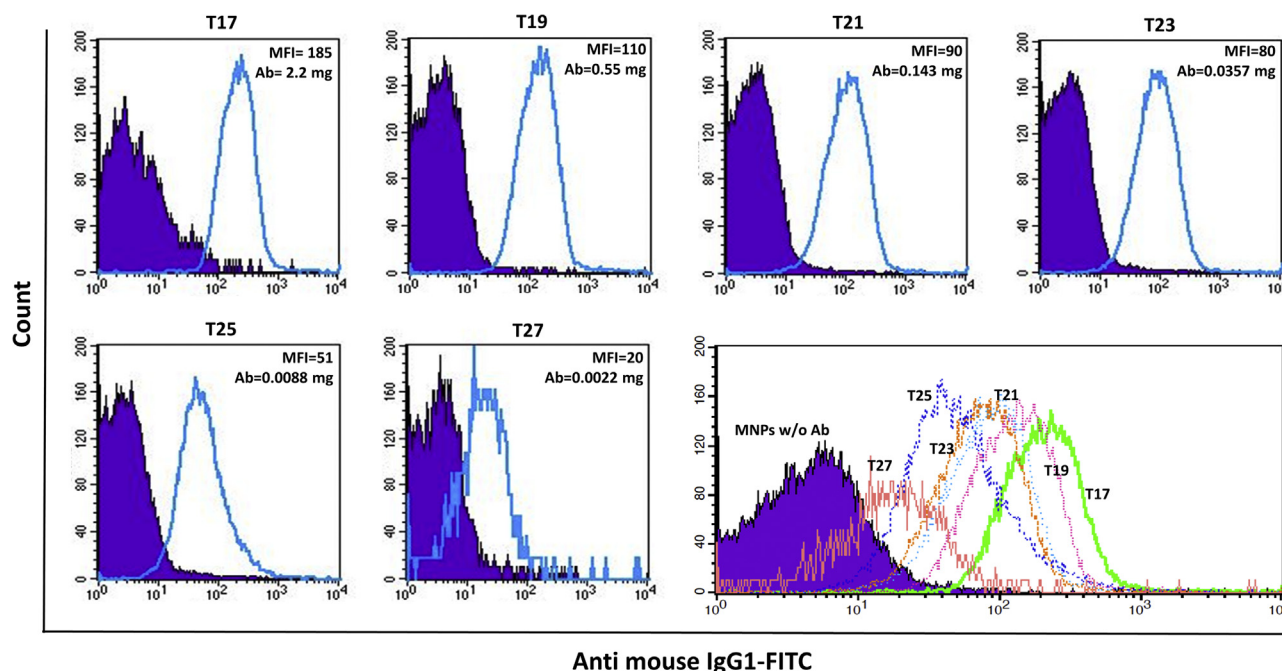
Figure 5. Flow cytometry diagrams of magnetic nanoparticles coated with different amounts of Herceptin. Stained samples (solid black line) were overlaid on the diagrams of magnetic nanoparticles without antibody (purple-filled). The samples were stained with FITC-conjugated mouse anti-human IgG1.

3. Results and discussion

3.1. Conjugation of Herceptin to MNPs

One of challenging issues in antibody binding on MNPs is the orientation of Abs on the MNP surface, which may be related to the conjugation strategy used. Covalent coupling through functional groups such as carbohydrates, thiols, amines or carboxyls is the most common method. To take advantage of carbohydrate chains in the Fc region of Abs, periodate-mediated oxidation has been used to target diols in carbohydrates and yield aldehyde groups. These aldehyde-activated groups can then react with functionalized MNPs, which contain primary amines. The lack of carbohydrates in some Abs and the need for modification, which may lead to oxidization of some other critical amino acids, are the main drawbacks associated with this method. In another method, free sulfhydryl groups are obtained by cleaving the disulfide-bridged cysteines positioned in the antibody hinge region, which subsequently react with maleimide- or iodoacetyl-activated MNPs. Because the tertiary structure of Abs comprises cysteine residues, despite high stability, antibody conjugation to MNPs with this method can disrupt antibody conformation [43, 44, 45].

One of the most popular alternative approaches for covalent attachment is the use of primary amine functional groups with lysine side chains. Amide bond formation involves the use of EDC/NHS as a cross-linking agent to provide coupling with MNPs bearing carboxylic groups on their surface. Despite high efficiency, because these amine groups are mostly located within the antigen binding sites, the main potential drawbacks are occupation of antigen-binding sites [46] and low conjugation rate of Abs through amide bonds (24–27%) [43]. It was previously shown that when carbodiimide was used to functionalize carboxyl groups in MNPs to bind to amine groups in Abs, the availability of antibody binding site was less than 10% [44]. For this reason, in the present study the reverse antibody binding method was chosen. In this method we initially activated the carboxyl groups of the Herceptin antibody in the Fc region with EDC/NHS, and then added amine-functionalized MNPs (Figure 1). With this approach we expected

antibody binding to MNPs to occur through their Fc regions, and consequently the Fab portions to remain active. After antibody conjugation by amide bands, the zeta potential of coated MNPs became more negative as a result of the reaction of amine groups in MNPs with carboxyl groups in Abs. As summarized in Table 2, the zeta potential of MNPs decreased from −72.6 to −56.4 when they were coated with silane, due to the amine groups in silane. This reduction was greater after Ab coating due to the interaction of negatively charged carboxylic group in the Abs with amino groups in MNPs. When larger amounts of antibody were tested (T17 compared to T25), the Ab-MNPs charge in sample T17 was more negative (−69.1 mV vs. −59.2 mV). Therefore, the change in zeta potential confirmed covalent bonding of the antibody to MNPs through amide bonds.

The FTIR results also confirmed Herceptin conjugation to MNPs. As shown in Figure 3 for sample T19, characteristic Fe–O bonds were detected at 580 and 640 cm^{-1} related to stretching vibration, and a bond at 1000–1100 cm^{-1} indicated asymmetric stretching vibration of the Si–O groups. Another characteristic broad peak at 3200-3600 cm^{-1} may represent hydroxyl and amine groups. The peak around 1640 cm^{-1} reflected the C=O bond and also antibody amide I; and the peak at 1546 cm^{-1} was assigned to the N–H bond of antibody amide II. These results confirmed covalent antibody binding to the MNP surface [39, 47, 48, 49].

EDX was also used to confirm antibody binding to the surface of MNPs. Because Herceptin is enriched for carbon (C), oxygen (O), nitrogen (N) and sulfur (S), we expected the EDX spectra of antibody-coated MNPs to contain higher percentages of these components compared to naked MNPs. As shown in Figure 4, the percentages of C, N, O and S in T17 were significantly higher than in naked MNPs (9.53, 6.52, 52.86, and 4.14 wt% vs. 4.6, 0, 40.07 and 1.04 wt%, respectively), suggesting successful antibody coating of the MNPs. Because of the larger numbers of antibody molecules on their surface, MNPs with a higher mean fluorescence intensity (MFI) were expected to have higher levels of C, N, O and S compared to those with lower MFI. To verify this assumption, the components of two samples, T17 (MFI = 185.56) and T19 (MFI = 110.19), were compared with EDX. As seen in Figure 4, the percentages of C, N, O and S were significantly lower in T19 than in T17 (7.19, 3.73, 45.83 and
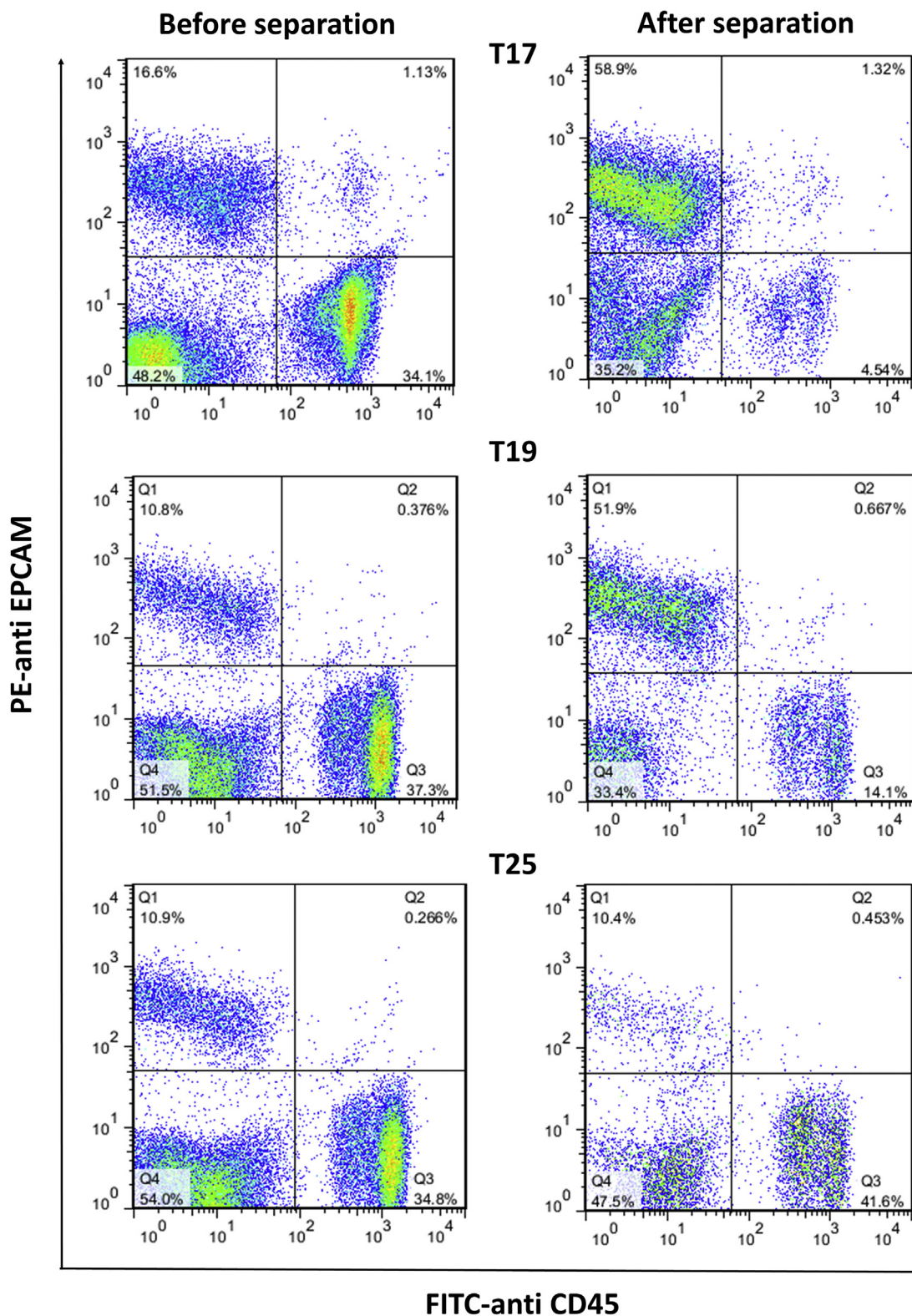
Figure 6. Flow cytometry analysis of SK-BR3 cell isolation from a mixture of peripheral blood mononuclear cells using magnetic nanoparticles coated with different amounts of Herceptin. **T17:** coated with 2.2 mg Herceptin, MFI = 185.56; **T19:** 0.55 mg Herceptin, MFI = 110.19; **T25:** 0.009 mg Herceptin, MFI = 51.75.

1.73 wt% vs. 9.53, 6.52, 52.86, and 4.14 wt%, respectively). The lower values in T19 indicated the presence of lower amounts of Abs on the surface of MNPs.

Most previous studies used a fixed amount of antibody for conjugation, and only their binding and isolation ability were reported without specifying the binding rate or efficiency. In the present study we used different amounts of Herceptin for reaction with fixed amount of MNPs in the same conditions (Table 1). In addition, a flow cytometry-based technique was used to quantitatively determine antibody conjugation to MNPs. In addition to analyzing antibody binding to MNPs, direct measures of the proportion of binding are also reported numerically here. For this purpose, an anti-human IgG1 antibody conjugated to FITC

6

Table 3. Efficiency of different antibody-conjugated magnetic nanoparticles in separating SK-BR-3 cells.

MNPs	MFI	Percentage of SK-BR-3 cells			Percentage of PBMCs	
		Before separation	After separation	Efficiency (%)	Before separation	After separation
T17	185.56	16.60	58.90	71.80	34.10	4.50
T19	110.19	10.80	51.90	79.20	37.30	14.10
T25	51.75	10.40	10.90	0.00	34.80	41.60

MNPs: magnetic nanoparticles, MFI: mean fluorescence intensity, PBMCs: peripheral blood mononuclear cells. T17: coated with 2.2 mg Herceptin; T19: coated with 0.55 mg; T25: coated with 0.009 mg Herceptin.
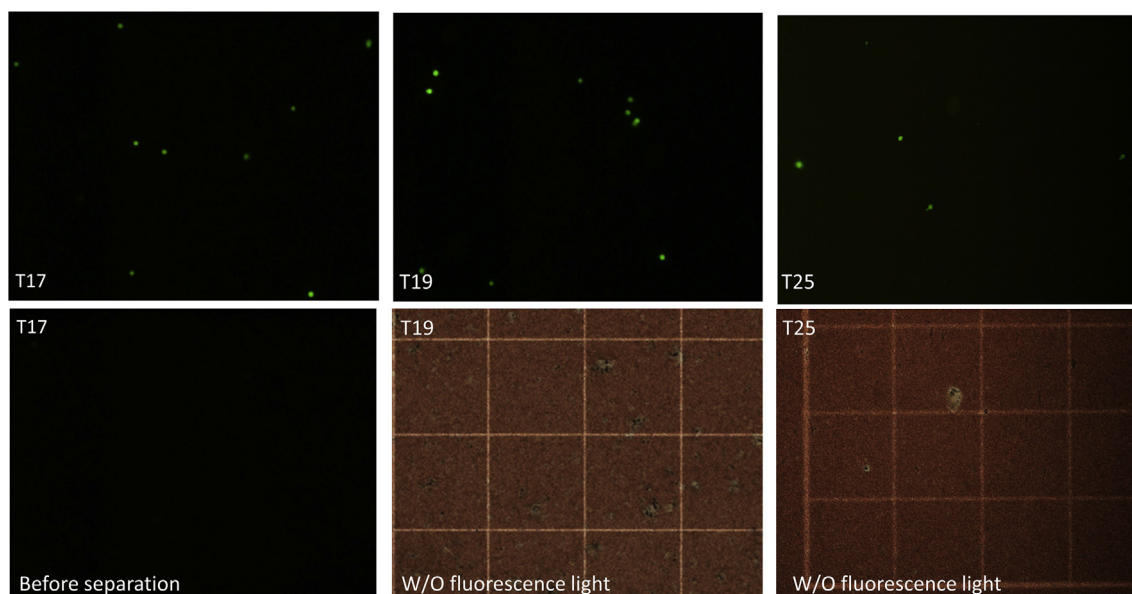
Figure 7. Fluorescence microscopy analysis of CFSC-labeled SK-BR-3 cells isolated from whole blood using magnetic nanoparticles coated with different amounts of Herceptin. **T17:** coated with 2.2 mg Herceptin, MFI = 185.56; **T19:** 0.55 mg Herceptin, MFI = 110.19; **T25:** 0.009 mg Herceptin, MFI = 51.75. All images were obtained at 10× magnification.

fluorescent dye was used to assess the conjugation of Herceptin to MNPs. The differences in MFI between labeled and unlabeled MNPs were considered a criterion for determining the efficiency of Herceptin coating. The diagrams (blue lines) for different samples with different MFI values are shown in Figure 5. To facilitate comparisons, purple-filled plots of MNPs without Herceptin are also shown in each panel. In all samples, even the lowest amount of Herceptin (0.002 mg) showed a shift in the geometric MFI for Herceptin-conjugated MNPs in comparison to negative controls (MNPs without Herceptin). The shifts demonstrated efficient antibody conjugation to MNPs in all quantities of Herceptin, though the binding rate decreased notably when the amount of antibody was reduced from 2.2 mg in T17 to 0.002 mg in T27. The highest MFI was 185.56 for T17, in which the largest amount of antibody was used, and the lowest MFI was 20.07 for T27, with the lowest concentration of antibody. Additionally, as summarized in Table 1 and Figure 5, when the ratio of MNPs to antibody increased from 0.79 to 795.45, antibody binding to MNPs decreased markedly, with the result that T27 plot almost completely overlaps the plot for MNPs without Herceptin. This result indicates that further reduction in the amount of antibody would be undesirable. In most previous studies the primary goal was anti-HER2 binding to the surface of MNPs; we were unable to find studies that reported the effect of different amounts of this antibody, although the binding of different amounts of other Abs to MNPs has been assayed in earlier work [13, 48]. In the present study different amounts of antibody ranging from very small to large were tested to determine the optimum antibody concentration for effective binding. Reducing the antibody

concentration in the binding reactions holds the potential to decrease the cost of developing these conjugates.

3.2. Isolation of SK-BR-3 cells with Herceptin-conjugated MNPs

We then evaluated the efficiency of MNPs with different amounts of antibody (different MFIs) in the separation of cells from PBMCs and blood cells. For this purpose, SK-BR-3, a breast cancer cell line, was selected as an example of HER2+ tumor cells. It has been reported that HER2 receptor expression on the surface of SK-BR-3 cells is more than 50- to 100-fold greater compared to normal cells [13]. Magnetic particles with different MFIs, i.e. T17 (MFI = 185.56), T19 (MFI = 110.19) and T25 (MFI = 51.75), were selected and added to a mixture of PBMCs and SK-BR-3 cells. After 2 h, HER2+ cells attached to Ab-MNPs were separated magnetically, and the isolation efficiency was evaluated with flow cytometry. At the same time control tubes were assayed with the same numbers of PBMCs, Ab-MNPs and SK-BR-3 cells but without further washing or magnetic sedimentation. To distinguish SK-BR-3 cells from PBMCs, we used specific Abs against human EpCAM, which are expressed on tumor cells, and also CD45 as a leukocyte marker. Flow cytometric analysis, as shown in Figure 6, showed that Herceptin-bound MNPs were able to separate cancer cells efficiently. Firstly, it showed that the antigen binding sites (Fab) in Herceptin were free and not occupied by MNPs, and MNPs were bound preferentially through the Fc region. In addition, a decrease in antibody levels from 2.2 mg in T17 to 0.55 mg in T19 had no

significant effect on Ab-MNP separation. The percentages of SK-BR-3 cells isolated by T17 and T19 were 58.9% and 51.9%, respectively (Table 3 and Figure 6), and the isolation yield in both experiments was similar (71.8 % and 79.2%, respectively). In T25, with a much lower antibody load compared to T17, Ab-MNPs had virtually no ability to separate SK-BR-3 cells from PBMCs. Accordingly, given that the MFI of T19 and T21 were similar, T21 appears to be a more appropriate choice rather than T17 for cell separation since T21 contained one-fifteenth the amount of antibody presents in T17. These results collectively show that Abs can be titrated to use the smallest amount able to efficiently separate target cells – a potential advantage especially for costly Abs. This possibility was confirmed in previous studies that tested different amounts of Abs to isolate target cancer cells [47].

3.3. Isolation of CFSC-stained SK-BR-3 cells from blood

In the next step, we tested the effect of different amounts of antibody on the separation efficiency of CFSE-labeled SK-BR-3 cells from peripheral blood. CFSE is a cell-permeable fluorescent dye which binds covalently to intracellular molecules through the succinimidyl group [50], and which stains labeled cells green under fluorescence microscopy. For this purpose, three different Ab-MNPs, T17, T19 and T25, were evaluated for their ability to separate cancer cells from blood. After separation in a magnetic field, isolated cells were detected under fluorescence microscopy.

Examination of the microscopic images showed that all MNPs were able to isolate SK-BR-3 cells in the magnetic field, albeit with different efficiencies (Figure 7). The images from all control samples (without magnetic separation) were dark, and no fluorescent cells were observed. The results of T19 and T17 were similar, but the numbers of SK-BR-3 cells isolated with T25 were less than 10% of the cells isolated with T19 or T17. These results are in line with our flow cytometry findings: in both experiments T19 and T17 MNPs, with an MFI of 110.19 and 185.56, respectively, performed much better than T25, with an MFI of 51.75. These results collectively confirmed the ability of MNPs to bind and separate cancer cells from blood.

4. Conclusion

To develop and optimize an immunomagnetic method for cell separation, we tested six different quantities of Abs bound through their carboxyl groups on amino-functionalized MNPs via EDC/NHS chemistry. The levels of conjugation, quantitatively characterized as MFI with flow cytometry, indicated that as the amount of Abs decreased, so did their binding on the surface of MNPs. The highest MFI measured in our samples was 185.56, and the lowest was 20.07, which corresponded respectively to T17 (2.2 mg) and T27 samples (0.002 mg). Assays of their target-binding abilities in blood and a mixture of lymphocytes and HER2+ SK-BR-3 breast cancer cells showed that MNPs with an MFI of 185.56 and 110.19 had similar separation efficiencies. However, the separation capacity of T25 (MFI = 50) was much lower, probably because of the lower amount of Abs conjugated with MNPs. These results were verified with fluorescence microscopy. Our findings showed that the optimal amount of Herceptin as an anti-HER2 antibody for conjugation with MNPs could be reduced from 2.2 mg to 0.143 mg (less than one-fifteenth) without compromising separation efficiency.

Declarations

Author contribution statement

Amir Hossein Haghighi: Conceived and designed the experiments; Performed the experiments; Analyzed and interpreted the data; Contributed reagents, materials, analysis tools or data; Wrote the paper.

Mohammad Taghi Khorasani: Analyzed and interpreted the data; Wrote the paper.

Zahra Faghih, Fatemeh Farjadian: Conceived and designed the experiments; Analyzed and interpreted the data; Contributed reagents, materials, analysis tools or data; Wrote the paper.

Competing interest statement

The authors declare no conflict of interest.

Additional information

No additional information is available for this paper.

References

[1] J. Kang, G. Yeom, H. Jang, J. Oh, C.-J. Park, M.-G. Kim, Development of replication protein A-conjugated gold nanoparticles for highly sensitive detection of disease biomarkers, Anal. Chem. 91 (15) (2019) 10001–10007.

[2] F. Fathian kolahkaj, K. Derakhshandeh, F. Khalesh, A.H. Azandaryani, K. Mansouri, M. Khazaei, Active targeting carrier for breast cancer treatment: monoclonal antibody conjugated epirubicin loaded nanoparticle, J. Drug Deliv. Sci. Technol. 53 (2019) 101136.

[3] H. Jahangirian, K. Kalantari, Z. Izadiyan, R. Rafiee-Moghaddam, K. Shameli, T.J. Webster, A review of small molecules and drug delivery applications using gold and iron nanoparticles, Int. J. Nanomed. 14 (2019) 1633–1657.

[4] Y.C. Kuo, H.C. Tsai, Rosmarinic acid- and curcumin-loaded polyacrylamide-cardiolipin-poly(lactide-co-glycolide) nanoparticles with conjugated 83-14 monoclonal antibody to protect β-amyloid-insulted neurons, Mater. Sci. Eng. C 91 (2018) 445–457.

[5] G.R. Han, M.G. Kim, Design, synthesis, and evaluation of gold nanoparticle-antibody-horseradish peroxidase conjugates for highly sensitive chemiluminescence immunoassay (hs-CLIA), Biothechnol Bioproc E 24 (1) (2019) 206–214.

[6] S. Glukhov, M. Berestovoy, P. Chames, D. Baty, I. Nabiev, A. Sukhanova, Quantification and imaging of HER2 protein using nanocrystals conjugated with single-domain antibodies, J Phys Conf Ser 784 (2017), 012016.

[7] F. Farjadian, A. Roointan, S. Mohammadi-Samani, M. Hosseini, Mesoporous silica nanoparticles: synthesis, pharmaceutical applications, biodistribution, and biosafety assessment, Chem. Eng. J. 359 (2019) 684–705.

[8] H.G. Jee, H.S. Ban, J.H. Lee, S.H. Lee, O.S. Kwon, J.H. Choe, Thermotherapy for Na+/I− symporter-expressing cancer using anti-Na+/I− symporter antibody-conjugated magnetite nanoparticles, J. Ind. Eng. Chem. 63 (2018) 359–365.

[9] K.R. Wu, H.H. Hsiao, Rapid and accurate quantification of amphetamine and methamphetamine in human urine by antibody decorated magnetite nanoparticles coupled with matrix-assisted laser desorption ionization time-of-flight mass spectrometer analysis, Anal. Chim. Acta 1025 (2018) 134–140.

[10] J.K. Xu, F.F. Zhang, J.J. Sun, J. Sheng, F. Wang, M. Sun, Bio and nanomaterials based on Fe3O4, Molecules 19 (12) (2014) 21506–21528.

[11] M. Bloemen, C. Denis, M. Peeters, L. De Meester, A. Gils, N. Geukens, et al., Antibody-modified iron oxide nanoparticles for efficient magnetic isolation and flow cytometric determination of L-pneumophila, Microchim Acta 182 (7-8) (2015) 1439–1446.

[12] M.I.J. Denison, S. Raman, N. Duraisamy, R.M. Thangavelu, S.U.M. Riyaz, D. Gunasekaran, et al., Preparation, characterization and application of antibody-conjugated magnetic nanoparticles in the purification of begomovirus, RSC Adv. 5 (121) (2015) 99820–99831.

[13] H. Xu, Z.P. Aguilar, L. Yang, M. Kuang, H. Duan, Y. Xiong, et al., Antibody conjugated magnetic iron oxide nanoparticles for cancer cell separation in fresh whole blood, Biomaterials 32 (36) (2011) 9758–9765.

[14] J. Xu, Q.M. Zhang, D.X. Zhao, Y.R. Liu, P. Chen, G.H. Lu, et al., High sensitive detection method for protein by combining the magnetic separation with cation exchange based signal amplification, Talanta 168 (2017) 91–99.

[15] Y. Xiao, C.H. Wang, X. Li, B. Wang, Research on magnetic separation methods for the extraction of nucleic acids, Adv. Mater. Res. 662 (2013) 343–347.

[16] Z. Ali, J. Wang, Y. Tang, B. Liu, N. He, Z. Li, Simultaneous detection of multiple viruses based on chemiluminescence and magnetic separation, Biomater Sci 5 (1) (2016) 57–66.

[17] L.L. Matta, E.C. Alocilja, Carbohydrate ligands on magnetic nanoparticles for centrifuge-free extraction of pathogenic contaminants in pasteurized milk, J. Food Protect. 81 (12) (2018) 1941–1949.

[18] X.-L. Gao, M.-F. Shao, Y.-S. Xu, Y. Luo, K. Zhang, F. Ouyang, et al., Non-selective separation of bacterial cells with magnetic nanoparticles facilitated by varying surface charge, Front. Microbiol. 7 (2016) 1891.

[19] N. Bohmer, N. Demarmels, E. Tsolaki, L. Gerken, K. Keevend, S. Bertazzo, et al., Removal of cells from body fluids by magnetic separation in batch and continuous mode: influence of bead size, concentration, and contact time, ACS Appl. Mater. Interfaces 9 (35) (2017) 29571–29579.

[20] A. Aires, S.M. Ocampo, B.M. Simoes, M. Josefa Rodriguez, J.F. Cadenas, P. Couleaud, et al., Multifunctionalized iron oxide nanoparticles for selective drug delivery to CD44-positive cancer cells, Nanotechnology 27 (6) (2016), 065103.

[21] D. Guo, G. Zhang, T.A. Wysocki, B.J. Wysocki, H.A. Gelbard, X.M. Liu, et al., Endosomal trafficking of nanoformulated antiretroviral therapy facilitates drug particle carriage and HIV clearance, J. Virol. 88 (17) (2014) 9504–9513.

[22] B.W. Tse, G.J. Cowin, C. Soekmadji, L. Jovanovic, R.S. Vasireddy, M.T. Ling, et al., PSMA-targeting iron oxide magnetic nanoparticles enhance MRI of preclinical prostate cancer, Nanomedicine 10 (3) (2015) 375–386.

[23] C.H. Sohn, S.P. Park, S.H. Choi, S.H. Park, S. Kim, L. Xu, et al., MRI molecular imaging using GLUT1 antibody-Fe3O4 nanoparticles in the hemangioma animal model for differentiating infantile hemangioma from vascular malformation, Nanomedicine: NBM (NMR Biomed.) 11 (1) (2015) 127–135.

[24] M.A. Tafoya, S. Madi, L.O. Sillerud, Superparamagnetic nanoparticle-enhanced MRI of Alzheimer's disease plaques and activated microglia in 3X transgenic mouse brains: contrast optimization, J. Magn. Reson. Imag. 46 (2) (2017) 574–588.

[25] F. Farjadian, S. Moradi, M. Hosseini, Thin chitosan films containing super-paramagnetic nanoparticles with contrasting capability in magnetic resonance imaging, J. Mater. Sci. Mater. Med. 28 (3) (2017) 47.

[26] D.C.F. Chan, D.B. Kirpotin, P.A. Bunn, Synthesis and evaluation of colloidal magnetic iron-oxides for the site-specific radiofrequency-induced hyperthermia of cancer, J. Magn. Magn Mater. 122 (1-3) (1993) 374–378.

[27] P. Zhang, Y. Zhang, M. Gao, X. Zhang, Dendrimer-assisted hydrophilic magnetic nanoparticles as sensitive substrates for rapid recognition and enhanced isolation of target tumor cells, Talanta 161 (2016) 925–931.

[28] S. Shanehsazzadeh, C. Gruettner, A. Lahooti, M. Mahmoudi, B.J. Allen, M. Ghavami, et al., Monoclonal antibody conjugated magnetic nanoparticles could target MUC-1-positive cells in vitro but not in vivo, Contrast Media Mol. Imaging 10 (3) (2015) 225–236.

[29] F.M. Kievit, Z.R. Stephen, O. Veiseh, H. Arami, T.Z. Wang, V.P. Lai, et al., Targeting of primary breast cancers and metastases in a transgenic mouse model using rationally designed multifunctional SPIONs, ACS Nano 6 (3) (2012) 2591–2601.

[30] F. Farjadian, A. Ghasemi, O. Gohari, A. Roointan, M. Karimi, M.R. Hamblin, Nanopharmaceuticals and nanomedicines currently on the market: challenges and opportunities, Nanomedicine 14 (1) (2019) 93–126.

[31] C.Y. Wen, Y.Z. Jiang, X.Y. Li, M. Tang, L.L. Wu, J. Hu, et al., Efficient enrichment and analyses of bacteria at ultralow concentration with quick-response magnetic nanospheres, ACS Appl. Mater. Interfaces 9 (11) (2017) 9416–9425.

[32] D.T. Ta, R. Vanella, M.A. Nash, Magnetic separation of elastin-like polypeptide receptors for enrichment of cellular and molecular targets, Nano Lett. 17 (12) (2017) 7932–7939.

[33] B. Saha, P. Songe, T.H. Evers, M.W.J. Prins, The influence of covalent immobilization conditions on antibody accessibility on nanoparticles, Analyst 142 (22) (2017) 4247–4256.

[34] A.H. Haghighi, Z. Faghih, M.T. Khorasani, F. Farjadian, Antibody conjugated onto surface modified magnetic nanoparticles for separation of HER2+ breast cancer cells, J. Magn. Magn Mater. 490 (2019) 165479.

[35] N.A. Byzova, I.V. Safenkova, E.S. Slutskaya, A.V. Zherdev, B.B. Dzantiev, Less is more: a comparison of antibody-gold nanoparticle conjugates of different ratios, Bioconjugate Chem. 28 (11) (2017) 2737–2746.

[36] B. Saha, T.H. Evers, M.W. Prins, How antibody surface coverage on nanoparticles determines the activity and kinetics of antigen capturing for biosensing, Anal. Chem. 86 (16) (2014) 8158–8166.

[37] S. Puertas, P. Batalla, M. Moros, E. Polo, P. Del Pino, J.M. Guisan, et al., Taking advantage of unspecific interactions to produce highly active magnetic nanoparticle-antibody conjugates, ACS Nano 5 (6) (2011) 4521–4528.

[38] Y.M. Huh, Y.W. Jun, H.T. Song, S. Kim, J.S. Choi, J.H. Lee, et al., In vivo magnetic resonance detection of cancer by using multifunctional magnetic nanocrystals, J. Am. Chem. Soc. 127 (35) (2005) 12387–12391.

[39] J.H. Almaki, R. Nasiri, A. Idris, F.A. Majid, M. Salouti, T.S. Wong, et al., Synthesis, characterization and in vitro evaluation of exquisite targeting SPIONs-PEG-HER in HER2+ human breast cancer cells, Nanotechnology 27 (10) (2016) 105601.

[40] M. Shamsipur, M. Emami, L. Farzin, R. Saber, A sandwich-type electrochemical immunosensor based on in situ silver deposition for determination of serum level of HER2 in breast cancer patients, Biosens. Bioelectron. 103 (2018) 54–61.

[41] K.R. Miller, A. Koide, B. Leung, J. Fitzsimmons, B. Yoder, H. Yuan, et al., T cell receptor-like recognition of tumor in vivo by synthetic antibody fragment, PloS One 7 (8) (2012) 43746.

[42] F. Farjadian, S. Ghasemi, S. Mohammadi-Samani, Hydroxyl-modified magnetite nanoparticles as novel carrier for delivery of methotrexate, Int. J. Pharm. 504 (1) (2016) 110–116.

[43] C. Gruttner, K. Muller, J. Teller, F. Westphal, A. Foreman, R. Ivkov, Synthesis and antibody conjugation of magnetic nanoparticles with improved specific power absorption rates for alternating magnetic field cancer therapy, J. Magn. Magn Mater. 311 (1) (2007) 181–186.

[44] R. Rezaeipoor, R. John, S.G. Adie, E.J. Chaney, M. Marjanovic, A.L. Oldenburg, et al., Fc-directed antibody conjugation of magnetic nanoparticles for enhanced molecular targeting, J Innov Opt Health Sci 2 (4) (2009) 387–396.

[45] S. Puertas, M. Moros, R. Fernández-Pacheco, M.R. Ibarra, V. Grazú, J.M. de la Fuente, Designing novel nano-immunoassays: antibody orientation versus sensitivity, J. Phys. D Appl. Phys. 43 (47) (2010) 474012.

[46] S. Jeong, J.Y. Park, M.G. Cha, H. Chang, Y.I. Kim, H.M. Kim, et al., Highly robust and optimized conjugation of antibodies to nanoparticles using quantitatively validated protocols, Nanoscale 9 (7) (2017) 2548–2555.

[47] H.M. Yang, C.W. Park, M.A. Woo, M.I. Kim, Y.M. Jo, H.G. Park, et al., HER2/neu antibody conjugated poly(amino acid)-coated iron oxide nanoparticles for breast cancer MR imaging, Biomacromolecules 11 (11) (2010) 2866–2872.

[48] K. Mu, S. Zhang, T. Ai, J. Jiang, Y. Yao, L. Jiang, et al., Monoclonal antibody-conjugated superparamagnetic iron oxide nanoparticles for imaging of epidermal growth factor receptor-targeted cells and gliomas, Mol. Imag. 14 (2015).

[49] Subodh, N.K. Mogha, K. Chaudhary, G. Kumar, D.T. Masram, Fur-Imine-functionalized graphene oxide-immobilized copper oxide nanoparticle catalyst for the synthesis of xanthene derivatives, ACS Omega 3 (11) (2018) 16377–16385.

[50] V. Lulevich, Y.-P. Shih, S.H. Lo, G.-Y. Liu, Cell tracing dyes significantly change single cell mechanics, J. Phys. Chem. B 113 (18) (2009) 6511–6519.